Generative Covert Communication: Leveraging Signal Coupling for Secret Data Transmission

Zhao Li, *Senior Member, IEEE,* Yanhong Xu, Linchuan Tan, Kang G. Shin, *Life Fellow, IEEE,* Yicheng Liu, *Student Member, IEEE,* Jia Liu, *Senior Member, IEEE,* Hanqing Ding, and Zheng Yan, *Fellow, IEEE*

***Abstract*—With the rapid advancement of communication technologies, wireless data transmissions have become pervasive. However, the open nature of the wireless medium makes these transmissions vulnerable to security threats, such as malicious detection and eavesdropping. Importantly, the prerequisite for these threats is the attackers' ability to detect the existence of legitimate transmissions. Covert communication (CovCom), a physical-layer security (PLS) technique designed to conceal legitimate transmissions from detection by attackers, serves as a fundamental security measure unlike other PLS schemes. Nevertheless, most existing CovCom schemes rely on covering signals that are independent of the covert signals themselves. This independence allows attackers to enhance their signal processing capabilities to separate the covert signal from the covering signal, ultimately extracting the original signal. Furthermore, the necessity for dedicated covering signal generation incurs additional power and hardware costs. To address these deficiencies, we propose a novel scheme called *Generative Covert Communication* (GCC), aimed at achieving covert data transmissions. GCC leverages interactions among covering signals; by adjusting their power and/or phases, a desired secret signal intended for the covert receiver (Rx) can be produced. Since the covert signals are derived from covering signals, they become coupled, and hence prevent attackers from decoupling them and detecting the existence of, as well as the content carried by, the secret transmissions. We design two GCC schemes: Power Control GCC (PC-GCC) and Phase Control GCC (ℙC-GCC). We utilize (1) the Universal Software Radio Peripheral (USRP) platform for experimental validation of GCC's feasibility and (2) comprehensive MATLAB simulations to demonstrate its effectiveness in achieving covert and secure data transmissions.**

***Index Terms*—Physical-layer security, covert communication, secure communication, power control, phase control**

I. Introduction

With the rapid development of 5G and the widespread adoption of the Internet of Things (IoT), a significant amount of sensitive user information — encompassing mobile payment transactions and health/medical information — is transmitted wirelessly, making the security of thus-transmitted information a critical concern for an increasing number of wireless applications. Due to the open nature of electromagnetic waves, wireless transmissions are susceptible to malicious detection and eavesdropping, which compromises data confidentiality and integrity [1].

Encryption [2] and physical-layer security (PLS) [3], [4] are two common approaches to safeguarding information security. However, both mechanisms primarily focus on securing transmitted content rather than concealing communication behaviors. In practice, adversaries typically begin by detecting target communication signals before launching jamming, eavesdropping, or spoofing attacks. Furthermore, even if attackers fail to demodulate legitimate user data, the mere detection of the legitimate signal may enable them to estimate the location of the signal source by estimating its direction and position [5], which, in turn, allows them to launch subsequent attacks. As a result, concealing communication behaviors has emerged as a key research challenge in the design of PLS.

Covert communication (CovCom) is a burgeoning wireless security technique designed to ensure reliable data transmission while preventing unauthorized entities from detecting the signal. In recent years, numerous CovCom approaches have been proposed [6]. Existing approaches can primarily be classified into two categories: (1) analyzing the performance limits of CovCom systems using information theory and designing coding methods with covert properties [7]–[9]; and (2) developing schemes that utilize artificial noise (AN) [10], [11], relay [12], and multi-antenna setups [13] to achieve effective covert transmission. The authors of [7] first derived a square root law (SRL) in an additive white Gaussian noise (AWGN) channel, laying the foundation for research into the theoretical performance limits of covert communication. To enhance the capacity of CovCom, the authors of [11] employed power-adjustable AN to modify the statistical characteristics of covert signals, thereby thwarting the warden's detection. A relay-assisted CovCom scheme was proposed in [12] where the relay amplifies the covert signal when necessary; otherwise, it transmits AN to disrupt the warden's detection. [13] utilized a multi-antenna jammer that transmits interference beams to disrupt warden's detection while confining the covert signal to the null space of the interference, thus ensuring covert communication performance.

However, existing CovCom approaches face several challenges. First, the covert Tx typically operates at reduced transmit power, thus limiting the achievable data rate at the covert Rx. Second, to degrade the warden's detection capabilities, additional resources such as transmit power, spectrum,

Zhao Li, Yanhong Xu, Linchuan Tan, Yicheng Liu, and Zheng Yan are with the School of Cyber Engineering, Xidian University, China. E-mail: zli@xidian.edu.cn; zyan@xidian.edu.cn.

Kang G. Shin is with the Department of Electrical Engineering and Computer Science, The University of Michigan, USA. E-mail: kgshin@umich.edu.

Jia Liu is with the Center for Strategic Cyber Resilience Research and Development, National Institute of Informatics, Japan. E-mail: jliu@nii.ac.jp. *(Corresponding author: Jia Liu)*

Hanqing Ding is with the School of Electronics and Information, Zhengzhou University of Light Industry, China. E-mail: dinghanqing@zzuli.edu.cn.

and hardware may be consumed [10]–[16], thus increasing resource overheads. Third, most CovCom schemes conceal covert signals within covering signals, such as AN [10], [11], background noise [14], and ambient communication signals [15], [16]. Since the covering signals are typically independent of the covert signals, attackers can enhance their signal processing capabilities to separate the covert signal from the covering signal, thus losing secrecy [17]. Therefore, it is critically important to develop CovCom schemes that mitigate/eliminate these deficiencies.

TABLE I
COMPARISON OF GCC WITH TYPICAL COVCOM APPROACHES.

Ref.	Key technique	Signal coupling	Power cost	Device overhead	Multi-antenna	Warden's location
[10]	AN	×	✓	✓	×	✓
[11]			✓	×	✓	×
[14]			×	×	×	✓
[16]			✓	×	✓	×
[12]	Relay	×	✓	✓	×	×
[13]	Multi-antenna	×	✓	✓	✓	×
[15]			×	×		
PC-GCC $\mathbb{F}$C-GCC	Signal Interaction	✓	×	×	✓	×

In this paper, we propose a Generative Covert Communication (GCC) method which leverages signal interactions and controls the power and/or phase of covering signals to facilitate covert and secure data transmissions. In GCC, existing communication signals are utilized as covering signals. By employing appropriate power and/or phase control, the characteristics of these covering signals are adjusted so that they can combine to produce a desired covert signal at the target Rx. GCC eliminates the need for additional hardware and reduces transmit power consumption. Moreover, since the covert signal is generated from the covering signals, they are coupled with each other, making it more difficult for attackers to decouple them and detect the existence of, as well as the content carried by, the covert transmissions. We design two GCC schemes: Power Control GCC (PC-GCC) and Phase Control GCC ($\mathbb{F}$C-GCC)[1]. These schemes implement GCC through power and phase control, respectively. Table I compares the proposed GCC with typical existing CovCom approaches, highlighting its advantages in terms of overhead, covertness, and secrecy/confidentiality.

Throughout this paper, we denote the set of complex numbers as $\mathbb{C}$, while vectors and matrices are represented by lower-case and upper-case bold letters. $(\cdot)^T$ and $(\cdot)^H$ represent matrix transpose and conjugate transpose, respectively, and $|\cdot|$ denotes the absolute value of a complex number.

II. SYSTEM MODEL

We consider a covert communication scenario depicted in Fig. 1, which consists of a Tx (Alice), a covering Rx (Bob)[2], a covert Rx (Carol), an eavesdropper (Eve), and a warden (Willie). The transmissions from Alice to Bob do not require security, while Alice aims to deliver covert information to Carol. Eve attempts to intercept and decode Alice's transmission to Carol, while Willie monitors signals transmitted from Alice to identify the existence of the communication from Alice to Carol. We denote the transmit power of Alice as P_T. Alice, Bob, Carol, Eve, and Willie are equipped with N_A, N_B, N_C, N_E, and N_W antennas, respectively.

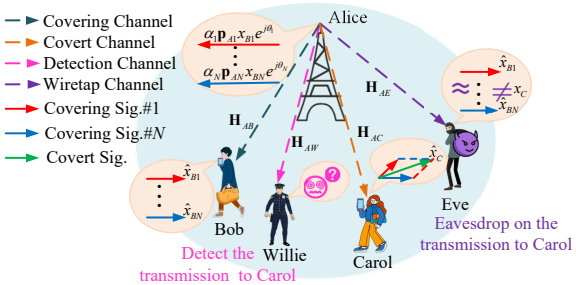

Fig. 1. System Model.

Let $\mathbf{H}_{AB} \in \mathbb{C}^{N_B \times N_A}$, $\mathbf{H}_{AC} \in \mathbb{C}^{N_C \times N_A}$, $\mathbf{H}_{AE} \in \mathbb{C}^{N_E \times N_A}$, and $\mathbf{H}_{AW} \in \mathbb{C}^{N_W \times N_A}$ denote the channel matrices from Alice to Bob, Carol, Eve, and Willie, respectively. We adopt a spatially uncorrelated Rayleigh flat fading channel to model the elements of the above channel matrices as independent and identically distributed (i.i.d.) zero-mean unit-variance complex Gaussian random variables. The channel follows a block fading characteristic, meaning the channel parameters remain constant in a block consisting of several successive time slots and vary randomly between successive blocks. Bob and Carol can estimate $\mathbf{H}_{AB}$ and $\mathbf{H}_{AC}$, respectively, and feed them back to Alice. Alice employs spatial multiplexing (SM) to transmit $N \leq \min\{N_A, N_B\}$ parallel spatial beams to Bob. Each beam is allocated equal power. We use the vector $\mathbf{x}_B = [x_{B1} \cdots x_{BN}]^T$ to represent the data sent from Alice and intended for Bob. The covert data that Alice intends to send to Carol is denoted by x_C. Alice pre-processes $\mathbf{x}_B$ using a precoding matrix $\mathbf{P}_A = [\mathbf{p}_{A1} \cdots \mathbf{p}_{AN}]$. To implement GCC, Alice must design a power control vector $\boldsymbol{\alpha} = [\alpha_1 \cdots \alpha_N]$ and/or a phase offset vector $\boldsymbol{\theta} = [\theta_1 \cdots \theta_N]$ to adjust the strengths and/or phases of the N spatial beams.

TABLE II
EVE'S CAPABILITY UNDER VARIOUS ADVERSARY MODELS.

Model	CSI knowledge		Signal processing method
	$\mathbf{H}_{AE}$	$\mathbf{H}_{AB}$	
I	✓	×	Single equivalent signal detection
II	✓	✓	Multiple spatial-domain signal detection

We consider Eve equipped with multiple antennas and relatively strong signal processing capabilities (i.e., $N_E \geq N$) as an example, primarily focusing on two typical adversary models, as shown in Table II. For adversary model I, since Eve cannot obtain $\mathbf{H}_{AB}$, she lacks knowledge of the spatial characteristics of the covering signals. Consequently, Eve processes the received mixed signal as a whole based on $\mathbf{H}_{AE}$. In model II, Eve can leverage sufficient CSI and her antenna

[1]For ease of differentiation, we use 'P' and '$\mathbb{F}$' to represent 'Power' and 'Ph' of 'Phase', respectively.

[2]Bob is the intended Rx of Alice. To distinguish him from the covert Rx, we refer to Bob as the covering Rx.

array to individually detect the covering signals in the spatial domain.

III. Design of Power Control GCC

We first present the design principle of Power Control GCC (PC-GCC), and then analyze its covertness and security.

A. Design of PC-GCC

Without loss of generality, we assume that Alice transmits to Bob and Carol using M-ary Phase Shift Keying (MPSK), setting $N_A = N_B = N_C = 2$ and $N_W = 1$. In these system settings, Alice employs SM to send $N = 2$ parallel data streams to Bob. We first present a general model of GCC, where both the power and phase of covering signals can be adjusted, encompassing both PC-GCC and $\mathbb{F}$C-GCC. Under this model, we allow Alice to control the two covering signals beams by adjusting their transmit powers via factors α_1 and α_2 (where $\alpha_1 + \alpha_2 = 1$) and their phases via θ_1 and θ_2. Then, the estimated filtered signal at Bob can be expressed as:

$$\begin{aligned}\hat{\mathbf{y}}_B &= \mathbf{F}_B^H \begin{bmatrix} \sqrt{\alpha_1 P_T} e^{j\theta_1} & 0 \\ 0 & \sqrt{\alpha_2 P_T} e^{j\theta_2} \end{bmatrix} \mathbf{H}_{AB} \mathbf{P}_A \mathbf{x}_B + \mathbf{F}_B^H \mathbf{n}_B \\ &= \begin{bmatrix} \sqrt{\alpha_1 P_T} e^{j\theta_1} \lambda_{B1} x_{B1} \\ \sqrt{\alpha_2 P_T} e^{j\theta_2} \lambda_{B2} x_{B2} \end{bmatrix} + \mathbf{F}_B^H \mathbf{n}_B. \end{aligned} \tag{1}$$

The first term on the right-hand side (RHS) of Eq. (1) represents the desired signal post-processed by Bob, where $\mathbf{x}_B = [x_{B1}\ x_{B2}]^T$ denotes the desired data for Bob, and $\mathbf{P}_A = [\mathbf{p}_{A1}\ \mathbf{p}_{A2}]$ is the precoding matrix employed by Alice. Taking precoding based on the singular value decomposition (SVD) as an example, we perform SVD on $\mathbf{H}_{AB}$ to obtain $\mathbf{H}_{AB} = \mathbf{U}_B \mathbf{\Sigma}_B \mathbf{V}_B^H = [\mathbf{u}_{B1}\ \mathbf{u}_{B2}] \begin{bmatrix} \lambda_{B1} & 0 \\ 0 & \lambda_{B2} \end{bmatrix} \begin{bmatrix} \mathbf{v}_{B1}^H \\ \mathbf{v}_{B2}^H \end{bmatrix}$. The two column vectors of $\mathbf{V}_B$ are adopted as the precoding vectors for $\mathbf{x}_B$, respectively, i.e., $\mathbf{p}_{A1} = \mathbf{v}_{B1}$ and $\mathbf{p}_{A2} = \mathbf{v}_{B2}$. Bob constructs his filter matrix as $\mathbf{F}_B = [\mathbf{f}_{B1}\ \mathbf{f}_{B2}] = [\mathbf{u}_{B1}\ \mathbf{u}_{B2}]$. $\mathbf{n}_B$ denotes the AWGN vector, whose elements have zero mean and variance σ_n^2.

In PC-GCC, only the transmit powers of the two covering signal beams are adjustable through factors α_1 and α_2, while the phases of the covering signals remain unchanged, i.e., $\theta_1 = \theta_2 = 0$. Substituting these parameters into Eq. (1) shows that power control in PC-GCC does not alter the spatial characteristics of the signals intended for Bob. Consequently, Bob's decoding is unaffected, and no modifications to Bob's reception are needed.

Carol's received signal under PC-GCC can be expressed as:

$$\mathbf{y}_C = \sqrt{\alpha_1 P_T} \mathbf{H}_{AC} \mathbf{p}_{A1} x_{B1} + \sqrt{\alpha_2 P_T} \mathbf{H}_{AC} \mathbf{p}_{A2} x_{B2} + \mathbf{n}_C, \tag{2}$$

where $\mathbf{n}_C$ is the AWGN vector at Carol. Carol employs $\mathbf{f}_C$ to post-process $\mathbf{y}_C$. The estimated signal can be written as:

$$\hat{\mathbf{y}}_C = \mathbf{f}_C^H \mathbf{y}_C = \sqrt{\alpha_1} s_{B1} + \sqrt{\alpha_2} s_{B2} + \mathbf{f}_C^H \mathbf{n}_C, \tag{3}$$

where both $\sqrt{\alpha_1} s_{B1}$ and $\sqrt{\alpha_1} s_{B2}$ ($s_{Bi} = \sqrt{P_T} \mathbf{f}_C^H \mathbf{H}_{AC} \mathbf{p}_{Ai} x_{Bi}$, $i \in \{1, 2\}$) are complex numbers. Then, for Carol to recover x_C from $\hat{\mathbf{y}}_C$, Eq. (4) must satisfy:

$$\sqrt{\alpha_1} s_{B1} + \sqrt{\alpha_2} s_{B2} = \varepsilon x_C, \tag{4}$$

where ε is a real-valued coefficient. As indicated by Eq. (4), the data recovered by Carol is the desired x_C scaled by ε. Since a complex-valued signal can be expressed in terms of its amplitude and phase, for simplicity, we define $x_i = \rho_i e^{j\varphi_i}$ where $i \in \{B1, B2, C\}$. ρ_i and φ_i represent the amplitude and phase of the signal, respectively.

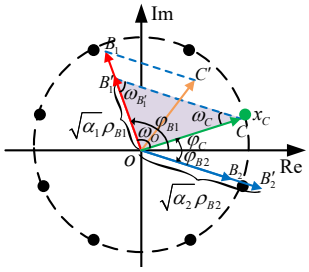

Fig. 2. Illustration of the power control in GCC.

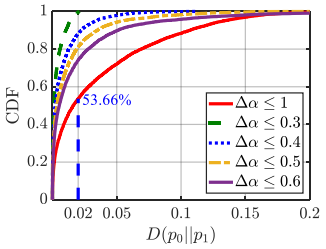

Fig. 3. CDFs of $D(p_0||p_1)$ with PC-GCC under different constraints.

Fig. 2 demonstrates that PC-GCC adjusts α_1 and α_2 to modify the superposition of s_{B1} and s_{B2}, thereby enabling Carol to retrieve x_C from her received mixed signals. We assume that Alice employs 8PSK to communicate with Bob and Carol, and, without loss of generality, that x_C is located in the first quadrant of the complex plane. In the figure, the complex numbers s_{B1}, s_{B2}, and x_C are represented by vectors $\overrightarrow{OB_1}$, $\overrightarrow{OB_2}$, and $\overrightarrow{OC}$, respectively. We define the range of the phase angle represented by a clockwise directional arc as $(-\pi, 0]$, and that of a counterclockwise directional arc as $(0, \pi]$. When there is no power control, the combination of s_{B1} ($\overrightarrow{OB_1}$) and s_{B2} ($\overrightarrow{OB_2}$) produces a resultant vector $\overrightarrow{OC'}$ whose phase deviates from that of x_C ($\overrightarrow{OC}$), resulting in a decoding error. By employing α_1 and α_2 to adjust the amplitudes of s_{B1} and s_{B2}, we achieve s'_{B1} ($\overrightarrow{OB'_1}$) and s'_{B2} ($\overrightarrow{OB'_2}$), which can produce the vector $\overrightarrow{OC}$ whose phase aligns with that of x_C. Thus, using PC-GCC, Alice can utilize covering signals intended for Bob to facilitate a data transmission to Carol.

We now present the method for solving α_1 and α_2. For simplicity, we use unidirectional arc ω_i ($i \in \{O, B'_1, C\}$) to represent the angle between two vectors. The range of ω_i is $[0, \pi)$. Based on our previous discussion, the amplitudes of s'_{B1} and s'_{B2} can be expressed as $\sqrt{\alpha_1}\rho_{B1}$ and $\sqrt{\alpha_2}\rho_{B2}$, respectively. They can superimpose to produce the estimated desired signal εx_C. Since Alice knows φ_{B1}, φ_{B2}, and φ_C, she can calculate $\omega_O = \varphi_{B1} - \varphi_C$. Moreover, in triangle $\triangle OB'_1C$, using the equality of alternate angles, we have $\omega_C = \varphi_C - \varphi_{B2}$. This leads to $\omega_{B'_1} = \pi - \omega_O - \omega_C = \pi - \varphi_{B1} + \varphi_{B2}$. Therefore, ω_O, $\omega_{B'_1}$, and ω_C can be calculated. Next, by applying the Law of Sines to triangle $\triangle OB'_1C$, we can obtain:

$$\sqrt{\alpha_1}\rho_{B_1} / \sin\omega_C = \varepsilon\rho_C / \sin\omega_{B'_1} = \sqrt{\alpha_2}\rho_{B_2} / \sin\omega_O. \tag{5}$$

Recall that $\alpha_1 + \alpha_2 = 1$, we can solve for α_1 and α_2 as:

$$\begin{cases} \alpha_1 = (\rho_{B2} \sin\omega_C)^2 / \left[(\rho_{B1} \sin\omega_O)^2 + (\rho_{B2} \sin\omega_C)^2\right] \\ \alpha_2 = (\rho_{B1} \sin\omega_O)^2 / \left[(\rho_{B1} \sin\omega_O)^2 + (\rho_{B2} \sin\omega_C)^2\right] \end{cases}. \tag{6}$$

Since Alice possesses the information of ρ_i ($i \in \{B1, B2, C\}$), she can determine α_1 and α_2 using Eq. (6). By following the above processing procedure, Alice can leverage covering signals in the environment to achieve a data transmission to Carol, without transmitting any dedicated signal to her. Since Willie can only detect the covering signals transmitted from Alice, and the covert transmission couples with these covering signals, he cannot detect the underlying communication to Carol, thereby ensuring covertness.

So far, we have presented the design of PC-GCC under $N = 2$. For $N > 2$, we can first partition them into two independent groups and perform signal superposition within each group to yield two equivalent covering signals. This allows for the direct application of the PC-GCC framework established in Fig. 2 and Eq. (6) to obtain two power factors associated with these equivalent covering signals. Finally, we map the computed power control factors proportionally to the covering signal components in each group. This way, PC-GCC is applicable to an arbitrary number of covering signals.

B. Covertness and Security Analysis of PC-GCC

1) Covertness Analysis of PC-GCC: PC-GCC achieves covertness via signal coupling. Willie's detection can be formulated as a binary hypothesis testing problem. His objective is to apply a decision rule to his observed signals to distinguish between $\mathcal{H}_0$ (the null hypothesis indicating that there is no transmission from Alice to Carol) and $\mathcal{H}_1$ (the alternative hypothesis indicating that Alice is transmitting a signal to Carol). Assuming equal prior probabilities for $\mathcal{H}_0$ and $\mathcal{H}_1$, Willie's detection performance is represented by the detection error probability $\xi = \Pr(\mathcal{D}_1|\mathcal{H}_0) + \Pr(\mathcal{D}_0|\mathcal{H}_1)$, where $\mathcal{D}_1$ and $\mathcal{D}_0$ indicates the decision regarding the presence and absence of communication from Alice to Carol, respectively.

From the perspective of covert communication, the transmission is considered covert if $\xi \geq 1 - \delta$, where $\delta \in [0, 1]$ is a predefined covertness coefficient. A smaller δ indicates a stricter covertness requirement. Conversely, Willie aims to minimize ξ to achieve covert signal detection. According to [7], [18], the lower bound of ξ can be derived as:

$$\xi = 1 - V_T(p_0, p_1) \geq 1 - \sqrt{0.5 \cdot D(p_0 \| p_1)}, \tag{7}$$

where $V_T(p_0, p_1)$ represents the total variation distance (TVD) between $p_0(y_W)$ and $p_1(y_W)$ which are the likelihood functions of the observed signal y_W at Willie under $\mathcal{H}_0$ and $\mathcal{H}_1$, respectively. $D(p_0\|p_1)$ denotes the Kullback-Leibler (KL) divergence between $p_0(y_W)$ and $p_1(y_W)$. By substituting $\xi \geq 1 - \delta$ into Eq. (7), we can derive the KL divergence-based covertness constraint as $D(p_0\|p_1) \leq 2\delta^2$.

Next, we calculate the KL divergence for PC-GCC. The observed signals at Willie can be expressed as:

$$y_W = \begin{cases} \sum_{i=1}^{N} \sqrt{P_T/N}\mathbf{H}_{AW}\mathbf{p}_{Ai}x_{Bi} + n_W, \ \mathcal{H}_0 \\ \sum_{i=1}^{N} \sqrt{\alpha_i P_T}\mathbf{H}_{AW}\mathbf{p}_{Ai}x_{Bi} + n_W, \ \mathcal{H}_1 \end{cases}. \tag{8}$$

From Eq. (9), we can obtain:

$$p_i(y_W) = (\pi\mu_i)^{-1} \exp\left(-|y_W|^2/\mu_i\right), \ i \in \{0, 1\}, \tag{9}$$

where $\mu_0 \triangleq \sum_{i=1}^{N} \frac{1}{N} P_T |\mathbf{H}_{AW}\mathbf{p}_{Ai}|^2 + \sigma_n^2$ and $\mu_1 \triangleq \sum_{i=1}^{N} \alpha_i P_T |\mathbf{H}_{AW}\mathbf{p}_{Ai}|^2 + \sigma_n^2$. σ_n^2 denotes the noise power at Willie.

We can then derive $D(p_0\|p_1)$ as:

$$D(p_0\|p_1) = \int_{-\infty}^{+\infty} p_0(y_W) \ln \frac{p_0(y_W)}{p_1(y_W)} dy = \ln \frac{\mu_1}{\mu_0} + \frac{\mu_0}{\mu_1} - 1. \tag{10}$$

Consequently, under $D(p_0\|p_1) \leq 2\delta^2$, we can calculate Carol's achievable covert data rate R_C as:

$$R_C = \log_2 \left(1 + \left|\sum\nolimits_{i=1}^{N} \sqrt{\alpha_i} s_{Bi}\right|^2 / \sigma_n^2\right). \tag{11}$$

where σ_n^2 represents the noise power at Carol.

2) Security Analysis of PC-GCC: In PC-GCC, the coupling characteristics between the covering and covert signals not only ensure covertness but also enhance resistance against eavesdropping. Under the adversary model I presented in Table II, Eve can only acquire $\mathbf{H}_{AE}$, processing the signals from Alice as a whole. Since Alice designs α_i where $i \in \mathcal{N} = \{1, \cdots, N\}$ based on $\mathbf{H}_{AC}$, and $\mathbf{H}_{AE}$ is independent of $\mathbf{H}_{AC}$, the filter vector derived by Eve from $\mathbf{H}_{AE}$ cannot aid in recovering x_C. Thus, confidentiality is guaranteed. Under adversary model II, Eve possesses both $\mathbf{H}_{AE}$ and $\mathbf{H}_{AB}$. By leveraging $\mathbf{H}_{AB}$, Eve can infer Alice's precoding matrix $\mathbf{P}_A$. Utilizing this knowledge, she can implement spatial signal processing to separate and decode the signal components from Alice, thereby recovering the data intended for Bob. However, it is important to note that the transmission of $\mathbf{x}_B$ does not have security requirements. As a result, the decoding of $\mathbf{x}_B$ may mislead Eve into falsely believing that she has successfully intercepted x_C, effectively functioning as a honeypot mechanism [19]. In summary, PC-GCC maintains secrecy under both adversary models.

IV. Design of Phase Control GCC

We first analyze the impact of power control on the covertness of PC-GCC and assess its feasibility, and then propose Phase Control GCC ($\mathbb{F}$C-GCC) to ensure both covertness and feasibility.

A. Impact of Power Control on the Covertness of PC-GCC

So far, PC-GCC has demonstrated that covert and secure data transmission can be achieved by implementing power control on covering signals. However, two key questions remain for further investigation: 1) Is power control sufficient to guarantee the feasibility of PC-GCC? and 2) Can Willie detect covert communication based on variations in power control factors? If yes, how can covertness be ensured? We will explore these two issues next.

As for the feasibility of GCC with only power control, as illustrated in Fig. 2, due to the randomness of x_C, when x_C falls outside the sector defined by the vectors s_{B1} and s_{B2}, there is no solution for $\boldsymbol{\alpha}$ that can yield appropriate s'_{B1} and s'_{B2} to produce x_C. Therefore, other adjustable signal

parameters must be considered in achieving GCC. To address this issue, we will propose $\mathbb{F}$C-GCC in the next subsection.

Concerning the impact of power control on the covertness of GCC, it is important to note that since $\boldsymbol{\alpha}$ modifies the strengths of covering signals, this results in a signal characteristics that differ from those without applying PC-GCC. Consequently, it is possible for Willie to detect the existence of covert communication by analyzing the statistical characteristics of the observed signal. Without loss of generality, we will consider equal power allocation for the covering signals as an example under $\mathcal{H}_0$. As mentioned before, $D(p_0||p_1)$ serves as a metric for covertness. According to Eq. (10), a more balanced power allocation, i.e., characterized by a smaller power allocation difference, defined as $\Delta\alpha = |\alpha_1 - \alpha_2|$, can result in a smaller $D(p_0||p_1)$, thus enhancing covertness.

Using MATLAB simulation, we analyze the impact of $\Delta\alpha$ on $D(p_0||p_1)$. We define $\zeta = 10\lg(P/\sigma_n^2)$dB, and set $\zeta = 10$dB in the simulation and use Monte Carlo simulations with 10^4 trials. In each trial, $\mathbf{H}_{AB}$, $\mathbf{H}_{AC}$, and $\mathbf{H}_{AW}$ are generated according to the configurations in Section II. Following [15], we set $D(p_0||p_1) \leq 0.02$ to ensure covertness. Fig. 3 illustrates the cumulative distribution function (CDF) curves of $D(p_0||p_1)$ for PC-GCC. As the figure shows, without restricting $\Delta\alpha$ (i.e., $\Delta\alpha \leq 1$), only 53.66% of the samples satisfy $D(p_0||p_1) \leq 0.02$. Then, we simulate the impact of $\Delta\alpha$ on $D(p_0||p_1)$ with $\Delta\alpha \in \{0.3, 0.4, 0.5, 0.6\}$ in Fig. 3. The results demonstrate that when $\Delta\alpha \leq 0.3$, the condition $D(p_0||p_1) \leq 0.02$ is satisfied. However, it is important to note that although restricting $\Delta\alpha$ can ensure covertness, it may degrade the feasibility of PC-GCC further. In the next subsection, we will propose $\mathbb{F}$C-GCC to address this issue.

B. Design of $\mathbb{F}$C-GCC

In $\mathbb{F}$C-GCC, Alice does not alter the strengths of the covering signals; instead, she selects a single covering signal to adjust its phase, referred to as the sacrificed covering signal (SCS), while keeping the other covering signals — called preserved covering signals (PCSs) — unchanged. Bob's detection of the PCSs is thus unaffected. The first issue in designing $\mathbb{F}$C-GCC is the selection of the SCS. It is necessary to fix the SCS for a communication period. This allows Bob to demodulate the PCSs without incurring excessive overhead from transmitting various SCS index information. To address this issue, we can select the covering signal with the minimum equivalent channel gain, specifically min $||\mathbf{H}_{AB}\mathbf{p}_{Ai}||$, as the SCS, thus maintaining the quality of the covering transmissions as much as possible. We denote the index of the SCS as n. Taking Alice's use of equal power allocation (i.e., $\alpha_i = 1/N$) as an example, the remaining $N-1$ PCSs are equivalent to an effective PCS, denoted as $s_{\Sigma PCS} = \sum_{i\in\mathcal{N}\backslash\{n\}} \sqrt{P_T/N}\mathbf{f}_C^H\mathbf{H}_{AC}\mathbf{p}_{Ai}x_{Bi}$, where $\mathcal{N}\backslash\{n\}$ represents $i \in \mathcal{N}$ and $i \neq n$. This effective PCS is then superimposed with the phase-adjusted SCS, expressed as $s_{SCS}e^{j\theta_{SCS}} = \sqrt{P_T/N}\mathbf{f}_C^H\mathbf{H}_{AC}\mathbf{p}_{An}x_{Bn}e^{j\theta_{SCS}}$, to yield the desired covert signal for Carol. Before detailing the design of $\mathbb{F}$C-GCC, we first present Lemma 1, which specifies the conditions for generating the covert signal.

Lemma 1: For any desired covert signal carrying x_C, if $|s_{SCS}| > |s_{\Sigma PCS}|$, then there exists a phase offset $\theta_{SCS} \in [0, 2\pi)$ such that the phase of the estimated superimposed signal $x'_C = s_{SCS}e^{j\theta_{SCS}} + s_{\Sigma PCS}$ satisfies $\arg(x'_C) = \arg(x_C)$.

The proof of Lemma 1 is provided in Appendix A.

According to Lemma 1, Carol can adopt a filter vector $\mathbf{f}_C$ to satisfy $|s_{SCS}| > |s_{\Sigma PCS}|$. For clarity, we define $\mathbf{g}_i = \mathbf{H}_{AC}\mathbf{p}_{Ai}$. Then, since $|x_{Bi}| = 1$, the condition $|s_{SCS}| > |s_{\Sigma PCS}|$ can be expressed as $|\mathbf{f}_C^H\mathbf{g}_n|^2 > |\sum_{i\in\mathcal{N}\backslash\{n\}} \mathbf{f}_C^H\mathbf{g}_i x_{Bi}|^2$, which leads to:

$$|\mathbf{f}_C^H\mathbf{g}_n|^2 > \sum\nolimits_{i\in\mathcal{N}\backslash\{n\}} |\mathbf{f}_C^H\mathbf{g}_i|^2 + \sum\nolimits_{i\in\mathcal{N}\backslash\{n\}} \sum\nolimits_{j\in\mathcal{N}\backslash\{i,n\}} (\mathbf{f}_C^H\mathbf{g}_i)(\mathbf{g}_j^H\mathbf{f}_C)(x_{Bi}x_{Bj}^*). \tag{12}$$

To satisfy Eq. (12), $\mathbf{f}_C$ must be calculated on a symbol-by-symbol basis, which is impractical. Therefore, we introduce a coefficient η and reformulate Eq. (12) into the following robust condition:

$$|\mathbf{f}_C^H\mathbf{g}_n|^2 > \eta \sum\nolimits_{i\in\mathcal{N}\backslash\{n\}} |\mathbf{f}_C^H\mathbf{g}_i|^2. \tag{13}$$

From Eq. (13), we can derive:

$$\mathbf{f}_C^H\mathbf{g}_n\mathbf{g}_n^H\mathbf{f}_C - \eta \sum\nolimits_{i\in\mathcal{N}\backslash\{n\}} \mathbf{f}_C^H\mathbf{g}_i\mathbf{g}_i^H\mathbf{f}_C > 0. \tag{14}$$

We then define a matrix $\mathbf{M} = \mathbf{g}_n\mathbf{g}_n^H - \eta\sum_{i\in\mathcal{N}\backslash\{n\}} \mathbf{g}_i\mathbf{g}_i^H$. Since $\mathbf{M} = \mathbf{M}^H$, it is a Hermitian matrix. Consequently, Eq. (14) can be reformulated as a problem of finding a vector $\mathbf{f}_C$ that satisfies $\mathbf{f}_C^H\mathbf{M}\mathbf{f}_C > 0$. Next, Lemma 2 provides the method for calculating $\mathbf{f}_C$ to satisfy $\mathbf{f}_C^H\mathbf{M}\mathbf{f}_C > 0$ (i.e., $|s_{SCS}| > |s_{\Sigma PCS}|$), which facilitates the calculation of θ_{SCS} according to Lemma 1, and the implementation of $\mathbb{F}$C-GCC.

Lemma 2: When $N_C \geq N$, selecting the eigenvector corresponding to the largest eigenvalue of $\mathbf{M}$ as $\mathbf{f}_C$ ensures that $|s_{SCS}| > |s_{\Sigma PCS}|$ holds, where $\eta \in [N-1, +\infty)$.

The proof of Lemma 2 can be found in Appendix B.

Once $\mathbf{f}_C$ is obtained, Alice configures θ_{SCS} for the SCS to satisfy $x'_C = s_{\Sigma PCS} + s_{SCS}e^{j\theta_{SCS}} = \varepsilon x_C$. To solve θ_{SCS}, we formulate a nonlinear optimization problem that minimizes the phase difference between x'_C and x_C, as $\min_{\theta_{SCS}\in[0,2\pi)} |\arg(x'_C) - \arg(x_C)|$. Numerical optimization tools, such as the *fmincon* function in MATLAB, can be employed to solve this optimization problem.

In conclusion, $\mathbb{F}$C-GCC achieves covert communication by adjusting the phase of only one covering signal.

C. Comparison of PC-GCC and $\mathbb{F}$C-GCC

We now compare PC-GCC and $\mathbb{F}$C-GCC in Table III. The PC-GCC relies solely on power control, but its power adjustments may incur a loss of covertness. Additionally, power control alone is insufficient to ensure the generation of the desired covert signal. In contrast, $\mathbb{F}$C-GCC adjusts only the phase of a single covering signal while keeping the remaining covering signals unchanged. This approach ensures

TABLE IV
PARAMETER SETTINGS OF PC-GCC.

Carrier freq.	Symbol rate	Interpolation factor	Sampling rate (base-band)	Roll-off factor of raised cosine filter	Transmit gain of each Tx
915MHz	0.2MBaud	2	0.4MBaud	0.5	[50dB,54dB]

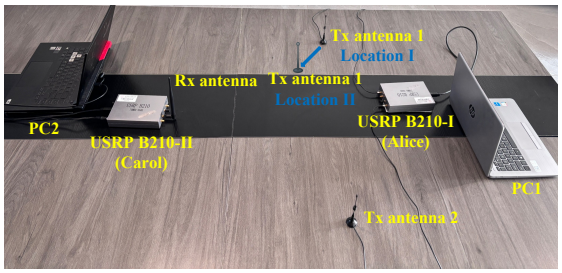

Fig. 4. Hardware implementation of PC-GCC.

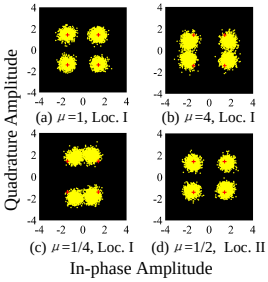

Fig. 5. Const. at Carol under various μs.

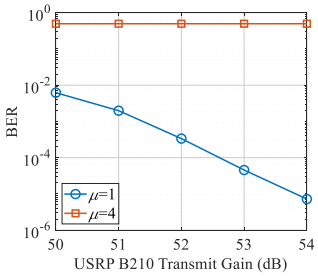

Fig. 6. BER of Carol under various μs.

both covertness and the availability of covert signal generation. More importantly, $\mathbb{F}$C-GCC does not modify the strengths of the covering signals; thus, the warden cannot detect the existence of covert communication based on variations in the powers of the covering signals. Furthermore, benefiting from phase adjustment, $\mathbb{F}$C-GCC can be applied not only to MPSK but also to Quadrature Amplitude Modulation (QAM), making it more versatile than PC-GCC. Specifically, in PC-GCC, while power control can facilitate the generation of the desired signal at Carol, it may conflict with the power allocation constraints necessary to ensure the covertness of Alice's transmission to Carol. As a result, PC-GCC is not applicable to QAM. In contrast, $\mathbb{F}$C-GCC can adjust the phases of multiple SCSs rather than just a single SCS, facilitating the generation of desired signal at Carol. However, as more SCSs are involved, the performance loss for the covering transmissions may become more pronounced.

TABLE III
COMPARISON OF PC-GCC AND $\mathbb{F}$C-GCC.

Comparison items	PC-GCC	$\mathbb{F}$C-GCC
Parameters for adjustment	Power	Phase
Number of covering signals for adjustment	N	1
Constraint on power control	×	N/A
Guarantee of covertness	×	✓
Guarantee of covert signal generation	×	✓
Number of affected covering signals	N	1
Extension to QAM	×	✓

V. EVALUATION

We first validate the feasibility of PC-GCC by implementing it on the Universal Software Radio Peripheral (USRP) platform. Subsequently, we evaluate the performance of both PC-GCC and $\mathbb{F}$C-GCC through MATLAB simulations.

A. Hardware Experiment

Fig. 4 illustrates our experimental setup. The aim of this experiment is to validate that the PC- GCC[3] enables Carol to successfully decode her data from the superposed covering signals. So, we focus on the adjustment of the covering signals transmitted from Alice and the decoding process at Carol, while omitting the transmission from Alice to Bob. In the experiment, Alice (the USRP B210-I connected to and controlled by terminal PC1) transmits two covering signals using BPSK[4] from her two transmit antennas, respectively. Meanwhile, Carol (the USRP B210-II connected to and controlled by terminal PC2) decodes her covert data using QPSK (i.e., the covert transmission adopts QPSK). The main parameters used in the experiment are summarized in Table IV.

As Fig. 4 shows, we initially deploy the two transmit antennas symmetrically (with transmit antenna 1 placed at Location I) with respect to Carol. In this setup, Carol is positioned on the perpendicular bisector of the line connecting the two transmit antennas. This configuration ensures that both covering signals experience nearly identical channel fading upon arrival at Carol, allowing for equal power allocation to produce the desired QPSK signal using the two BPSK covering signals. Subsequently, we move transmit antenna 1 to Location II, resulting in different fading conditions for the two covering signals when they arrive at Carol. In this case, we need to select appropriate values for α_i (where $i \in \{1, 2\}$) to generate the desired QPSK signal. At the Rx side, Carol, who has a single antenna, first estimates the equivalent channel state between herself and Alice based on the reception of a predefined pilot sequence sent by Alice. In our experiment, we use a Barker code for synchronization and channel estimation. Following this estimation, Carol performs channel compensation, which includes correcting for frequency and phase offsets, as well as applying automatic gain control (AGC), before demodulating the superimposed signal using QPSK decoding. Note that the transmit power of each antenna of Alice (i.e., USRP B210-I) is jointly determined by the amplitude of the baseband signal and the transmit gain of the USRP device [20]. To investigate the impact of power control factors on the quality of the superimposed signal at Carol, we set the transmit gain of both antennas of Alice to be identical and adjust the amplitudes[5] of the two baseband signals in the

[3]Since the phase control is difficult to implement in this experiment, we leave the evaluation of $\mathbb{F}$C-GCC for Section V-B.

[4]One BPSK modulation utilizes the phase set $\{0, \pi\}$ while the other uses $\{\pi/2, 3\pi/2\}$.

[5]The power control factor is the square of the amplitude of the baseband signal.

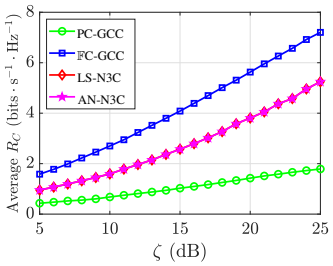

Fig. 7. Comparison of average R_C under various methods with $N = N_C = 2$.

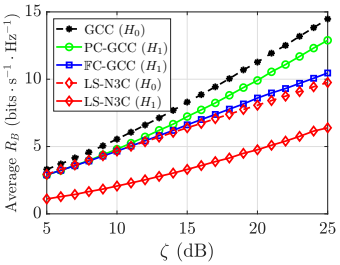

Fig. 8. Comparison of R_B under various methods with $N_A = N_B = N = 2$.

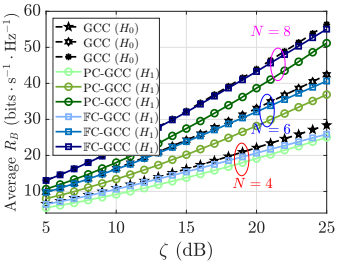

Fig. 9. Comparison of R_B under various methods with $N_A = N_B = N \in \{4, 6, 8\}$.

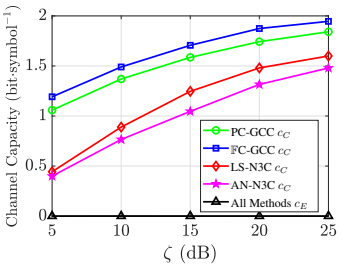

Fig. 10. Variation of c_C and c_E with ζ under $N = N_C = N_E = 2$ and adversary model I assumption.

digital domain, ensuring that the total transmit power of Alice remains constant.

We define the ratio of α_1 to α_2 as μ. Fig. 5 illustrates the constellation map at Carol under various μs. As the figure shows, when antenna 1 is positioned at Location I, the two covering signals undergo similar channel fading. Therefore, setting $\mu = 1$ yields a standard QPSK constellation (indicating successful generation of the desired signal) at Carol, as depicted in subplot (a). In contrast, when $\mu = 4$ and $\mu = 1/4$, Carol can only observe an attenuated QPSK constellation (indicating failure to generate the desired signal) due to inappropriate power control factors at Alice, as shown in subplots (b) and (c). When antenna 1 is moved to Location II, the two covering signals experience different fading conditions. By setting $\mu = 1/2$, Carol can again observe a standard QPSK constellation. In conclusion, Fig. 5 demonstrates that with proper power control, the covering signals can produce the desired signal at Carol.

To further evaluate the impact of power control on Carol's reception performance, we analyze the bit-error rate (BER) of Carol under $\mu \in 1, 4\}$. In this experiment, antenna 1 is placed at Location I. As shown in Fig. 6, when $\mu = 1$, Carol's BER decreases significantly as the transmit gain of USRP B210-I device increases. This improvement occurs because, under $\mu = 1$, the covering signals can superimpose to generate a high-quality desired signal at Carol, resulting in accurate demodulation. Conversely, when $\mu = 4$, Carol's BER remains consistently around 50%. This is due to the inappropriate power control factors preventing the correct combination of the covering signals at Carol, resulting in a distorted signal and decoding errors. In summary, the experimental results demonstrate the effectiveness of PC-GCC.

B. MATLAB Simulation

We now evaluate the performance of both GCC methods through MATLAB simulations. In the simulations, both Alice and Bob are equipped with $N_A = N_B = N \in \{2, 4, 6, 8\}$ antennas, while Carol has $N_C \in \{2, 4, 6, 8\}$ antennas and Eve has $N_E = 2$ antennas. We set $\zeta \in [5, 25]$dB. Alice employs QPSK for data transmission. All other parameters remain consistent with those in Section IV-A.

To demonstrate the superiority of the proposed GCC methods, which utilize signal coupling for CovCom, we compare them against two non-coupling CovCom (N3C) methods for comparison: legitimate signal-aided N3C (LS-N3C) [15] and AN-aided N3C (AN-N3C) [16]. In LS-N3C, the legitimate transmission from Alice to Bob serves as the covering signal, while AN-N3C uses artificial noise as the covering signal. However, the covert signal in both methods is generated independently without coupling with the covering signal. Moreover, in LS-N3C, we employ zero-forcing reception at the Rxs to mitigate co-channel interference, while in AN-N3C, we design the signature of AN to avoid interference with the covert transmission. In the simulations for these methods, we restrict the total transmit power to P_T and also consider the covertness constraint discussed in Section IV-A, formulating an optimal power allocation problem to maximize R_C.

Fig. 7 compares the average R_C for various schemes. In the simulation, when the transmission from Alice to Carol fails to establish, we count R_C as zero. As the figure shows, PC-GCC achieves the lowest average R_C among all methods, which is attributed to its high likelihood of unavailability in covert signal generation. In contrast, the other schemes ensure successful covert signal generation, resulting in superior average R_C. Specifically, $\mathbb{F}$C-GCC achieves the highest average R_C, while both N3C methods achieve similar R_C values that are lower than those of $\mathbb{F}$C-GCC. This difference arises because $\mathbb{F}$C-GCC does not incur any additional power cost, as the covert transmission directly utilizes the covering signals. In contrast, both N3C methods must consume some transmit power for covering signal transmissions, which reduces the available power for covert transmission, leading to their lower average R_C.

Fig. 8 illustrates the impact of CovCom on the average data rate of the covering transmissions, denoted as average R_B, under various schemes. Under $\mathcal{H}_0$, there is only communication between Alice and Bob, which we label as 'GCC ($\mathcal{H}_0$)' in the figure. For the two GCC methods, their R_B is the sum of the rates from $N = 2$ covering data transmissions. Note that AN-N3C utilizes AN as covering signal, resulting in $R_B = 0$. Therefore, we do not plot the R_B curve for AN-N3C. As the figure shows, the average R_B for the two GCC methods under $\mathcal{H}_1$ decreases compared to that under GCC ($\mathcal{H}_0$). Among them, PC-GCC exhibits a smaller reduction in R_B. This is because PC-GCC only adjusts the powers of the covering signals while keeping their phases unchanged, resulting in relatively minor degradation of covering communication performance under phase modulation scheme when

CovCom is present. In contrast, $\mathbb{F}$C-GCC adjusts the phase of a single covering signal while leaving the other covering signals unaltered, thereby preserving one reception for Bob while degrading the other, leading to a more significant R_B loss than PC-GCC. Additionally, LS-N3C experiences a noticeable degradation in average R_B when CovCom is present. This degradation is more severe than that incurred by the two GCC methods due to power consumption for covert signal transmission, which reduces the available power for covering communications.

Fig. 9 further demonstrates the impact of CovCom on the average R_B under various Ns. As the figure shows, $\mathbb{F}$C-GCC has a minimal impact on R_B across these N values, benefiting from its phase adjustment of only a single covering signal. Moreover, as N increases, the loss of average R_B progressively diminishes. In comparison, the degradation of R_B under PC-GCC is more pronounced, as PC-GCC modifies the strengths of all covering signals, leading to an accumulated and noticeable reduction in R_B. In summary, $\mathbb{F}$C-GCC is advantageous over PC-GCC in preserving covering communication performance, especially when N is larger.

Next, we evaluate the channel capacity for Carol and Eve, denoted as c_C and c_E, respectively, under various transmission schemes. We utilize the maximum average mutual information [21] as the metric for evaluating c_C and c_E. Fig. 10 plots the variation of c_C and c_E along with ζ. We consider adversary model I as an example. Under these conditions, Eve can attempt to demodulate the received mixed signal for interception. Since the N3C methods use either a communication signal or AN as the covering signal, they can also provide some anti-eavesdropping capabilities. Given that we assume Alice uses QPSK for data transmission, the maximum achievable capacity in this simulation is 2 bits/symbol. As the figure shows, c_C for all methods monotonically increases as ζ increases, approaching 2 bits/symbol as ζ becomes sufficiently large. However, the GCC methods outperform the N3C schemes in terms of c_C, as the latter must allocate some transmit power for covering signal transmission, which reduces the power available for communication to Carol. Furthermore, c_C for $\mathbb{F}$C-GCC exceeds that of PC-GCC. This is because $\mathbb{F}$C-GCC can generate a higher-quality desired covert signal than PC-GCC, resulting in a greater c_C. Regarding c_E, all methods yield identical results of zero. This is due to the covertness constraint, which ensures a strong enough covering signal to significantly degrade the signal-to-interference-plus-noise ratio (SINR) at Eve and leads to her decoding failure. For simplicity, we plot only one curve to represent c_E for all methods.

For adversary model II, even if Eve obtains both $\mathbf{H}_{AB}$ and $\mathbf{H}_{AE}$, enabling her to deduce Alice's precoding matrix $\mathbf{P}_A$ and recover $\mathbf{x}_B$ when GCC methods are applied, since Eve lacks knowledge of $\mathbf{H}_{AC}$, the generation of the covert signal from covering signals remains transparent to her. Additionally, due to the statistical independence between $\mathbf{x}_B$ and x_C, Eve cannot infer any information about x_C from the decoded $\mathbf{x}_B$, thus achieving effective eavesdropping resistance. Regarding the N3C methods, Eve's knowledge of $\mathbf{H}_{AB}$ cannot assist her in intercepting the date intended for Carol. Consequently, a zero value of c_E is yielded. Furthermore, the choice of adversary model does not affect c_C. As a result, the simulation results under adversary model II are identical to those presented in Fig. 10. Therefore, we only include Fig. 10 to avoid redundancy.

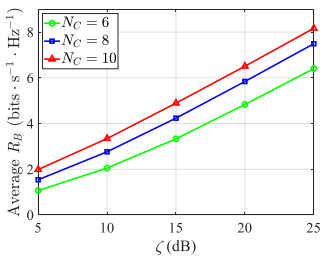

Fig. 11. Variation of R_C with ζ under $N_A = N_B = N = 6$, $\eta = 5$, and $N_C \in \{6, 8, 10\}$.

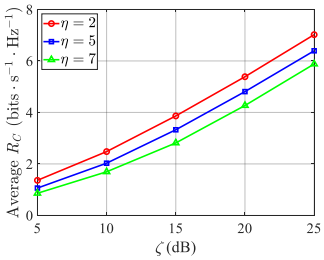

Fig. 12. Variation of R_C with ζ under $N_A = N_B = N = N_C = 6$ and $\eta \in \{2, 5, 7\}$.

On the premise that $N_C \geq N$, we proceed to investigate the impact of N_C on R_C under $\mathbb{F}$C-GCC. In Fig. 11, we simulate the variation of R_C with ζ under $N_A = N_B = N = 6$, $\eta = 5$, and $N_C \in \{6, 8, 10\}$. As the figure shows, R_C increases as N_C increases. This improvement arises from Carol's enhanced spatial processing capabilities with a larger N_C. Specifically, as N_C grows, $\mathbf{g}_n$ and $\{\mathbf{g}_i\}_{i \neq n}$ exhibit orthogonal relationships. This enables $\mathbf{f}_C$ to be align with $\mathbf{g}_n$ while maintaining near-orthogonality with $\{\mathbf{g}_i\}_{i \neq n}$, allowing the synthesized signal to be dominated by the SCS component. Moreover, increasing N_C results in a greater array gain, directly enhancing $|\mathbf{f}_C^H \mathbf{g}_n|^2$ and subsequently improving R_C.

Fig. 12 further illustrates the variation of R_C with ζ under $N_A = N_B = N = N_C = 6$ and various ηs[6]. As the figure shows, decreasing η enhances R_C. This is because, when η is small, the influence of $\{\mathbf{g}_i\}_{i \neq n}$ on the calculation of $\mathbf{f}_C^H \mathbf{M} \mathbf{f}_C$ is weakened. This results in the availability of $\mathbf{f}_C$ aligning with the SCS component $\mathbf{g}_n$, thereby enhancing the term $|\mathbf{f}_C^H \mathbf{g}_n|^2$ and consequently R_C. In contrast, as η increases, $\mathbf{f}_C$ transitions to a zero-forcing filter, becoming orthogonal to $\{\mathbf{g}_i\}_{i \neq n}$. This creates a mismatch between $\mathbf{f}_C$ and $\mathbf{g}_n$, leading to a decrease in $|\mathbf{f}_C^H \mathbf{g}_n|^2$ and R_C.

VI. Conclusion

In this paper, we explore the interactions among covering signals and, by adjusting their powers and/or phases, generate the desired covert transmission. We have proposed two GCC methods: PC-GCC and $\mathbb{F}$C-GCC. By leveraging the coupling relationships between the covering and covert signals, our proposed methods can cooperatively provide covertness and secrecy for data transmissions without incurring additional power or hardware overhead. Specifically, $\mathbb{F}$C-GCC balances

[6]Note that in the simulation, we can set $\eta = 2 < N - 1$, which does not conform to Lemma 2. This is because the requirement for $\eta \geq N - 1$ in Lemma 2 is to ensure $|s_{SCS}| > |s_{\Sigma PCS}|$ in all cases. However, according to the proof of Lemma 2, this requirement is beyond the actual need. As a result, $\eta = 2$ is sufficient for the $\mathbb{F}$C-GCC to achieve a feasible probability of 1.

the efficiency of covering communications with the performance of covert transmissions, achieving overall superior performance compared to PC-GCC. Our theoretical analysis, hardware experiments, and numerical simulations validate the feasibility of the two GCC methods and demonstrate their effectiveness in ensuring covertness and secure data transmissions compared to other typical PLS schemes.

ACKNOWLEDGMENTS

This work is supported in part by the National Natural Science Foundation of China under Grant 62072351, Grant U23A20300, Grant 62202359, in part by the 111 Center under Grant B16037, in part by JSPS KAKENHI under Grant JP25K15087, in part by the Science and Technology Research Project of Henan Province under Grant 252102211120, in part by the Project of Cyber Security Establishment with Inter-University Cooperation, in part by the Key Research Project of Shaanxi Natural Science Foundation under Grant 2023-JC-ZD-35, and in part by the U.S. National Science Foundation under Grant 2245223.

APPENDIX A
PROOF OF LEMMA 1

First, we illustrate in Fig. 13 the complex quantities mentioned in Lemma 1 in a geometric manner. As the figure shows, we use vectors $\overrightarrow{OP}$ and $\overrightarrow{OS}$ to denote $s_{\Sigma PCS}$ and s_{SCS}. The desired covert data x_C is represented by the vector, whose phase is θ_C. The superposition of $\overrightarrow{OP}$ and the phase-adjusted vector $\overrightarrow{OS'}$ is denoted by x'_C. x'_C lies on a circle centered at point P with radius of $|s_{SCS}|$. The subsequent discussions are based on the relationship between $|s_{SCS}|$ and $|s_{\Sigma PCS}|$.

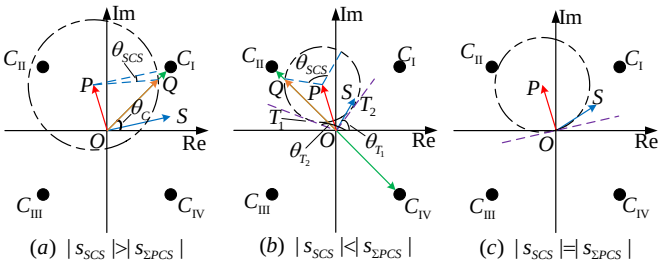

Fig. 13. Various superpositions of covering signals.

1) $|s_{SCS}| > |s_{\Sigma PCS}|$: As illustrated in subplot (a), $|s_{SCS}| > |s_{\Sigma PCS}|$ indicates that the origin is located inside circle P. Consequently, any vector originating from the origin with an arbitrary phase θ_C will inevitably intersect circle P. Let the intersection point be Q; then, the vector $\overrightarrow{OQ}$ represents a possible x'_C. Moreover, since Q lies on circle P, there exists a specific angle θ_{SCS} such that $\overrightarrow{OQ} = \overrightarrow{OP} + \overrightarrow{OS} \cdot e^{j\theta_{SCS}}$. Therefore, the phase of x'_C, denoted as $\arg(x'_C)$, satisfies $\arg(x'_C) = \arg(x_C) = \theta_C$.

2) $|s_{SCS}| \leq |s_{\Sigma PCS}|$: This condition indicates that the origin O is either outside or on circle P. As illustrated in subplots (b) and (c), in both scenarios, neither $\arg(x'_C)$ nor the circle P is able to cover all four quadrants, resulting in the generation of x_C being unavailable in these uncovered areas.

Therefore, to ensure successful covert signal generation, we adopt the condition $|s_{SCS}| > |s_{\Sigma PCS}|$. Consequently, Lemma 1 follows. ■

APPENDIX B
PROOF OF LEMMA 2

The proof of Lemma 2 consists of two parts. First, we verify that when $N_C \geq N$, the maximum eigenvalue of the matrix $\mathbf{M}$, denoted as τ_M, is greater than 0, ensuring the existence of a filter vector $\mathbf{f}_C$ satisfying $\mathbf{f}_C^H \mathbf{M} \mathbf{f}_C > 0$. Then, we will demonstrate that when $\mathbf{f}_C$ is the eigenvector of $\mathbf{M}$ corresponding to τ_M (denoted as $\mathbf{e}_M$) and $\eta \geq N-1$ holds, the condition $|s_{SCS}| > |s_{\Sigma PCS}|$ is guaranteed. Given below is the detailed proof.

1) Proof of $\tau_M > 0$: When $N_C \geq N$, $\text{rank}(\mathbf{H}_{AC}) = N$ holds, indicating that $\mathbf{H}_{AC}$ is of full column rank, and its null space contains only the zero vectors. This ensures linear independence among $\mathbf{g}_i$s. In this situation, we can construct a vector $\mathbf{f}_C$ that satisfies $\mathbf{f}_C^H \mathbf{M} \mathbf{f}_C > 0$. Define the subspace spanned by the PCSs as $\boldsymbol{\mathcal{I}} = \text{span}\{\mathbf{g}_i\}_{i \neq n}$, where span$\{\}$ denotes the subspace spanned by the vectors in the set $\{\}$. Since $\mathbf{g}_n \notin \boldsymbol{\mathcal{I}}$, its component being orthogonal to $\boldsymbol{\mathcal{I}}$, denoted as $\mathbf{g}_n^\perp$, is non-zero. Then, by letting $\mathbf{f}_C = \mathbf{g}_n^\perp$, we get $\mathbf{f}_C^H \mathbf{M} \mathbf{f}_C = (\mathbf{g}_n^\perp)^H \left(\mathbf{g}_n \mathbf{g}_n^H - \eta \sum_{i \in \mathcal{N} \setminus \{n\}} \mathbf{g}_i \mathbf{g}_i^H \right) \mathbf{g}_n^\perp = \|\mathbf{g}_n^\perp\|^4 > 0$. Since $\mathbf{f}_C^H \mathbf{f}_C = \|\mathbf{f}_C\|^2$ is positive, according to the Rayleigh-Ritz theorem [22], we can have:

$$\tau_M \geq (\mathbf{f}_C^H \mathbf{M} \mathbf{f}_C)/(\mathbf{f}_C^H \mathbf{f}_C) > 0. \tag{15}$$

Thus, we complete the proof that $\tau_M > 0$ when $N_C \geq N$.

2) Proof of $|s_{SCS}| > |s_{\Sigma PCS}|$: The condition $|s_{SCS}| > |s_{\Sigma PCS}|$ is equivalent to $|\mathbf{f}_C^H \mathbf{g}_n x_{Bn}|^2 > |\sum_{i \in \mathcal{N} \setminus \{n\}} \mathbf{f}_C^H \mathbf{g}_i x_{Bi}|^2$. Considering the worst-case scenario where all PCS components are in-phase superimposed (yielding the maximum modulus of $|s_{\Sigma PCS}|$), we can simplify this to $\left|\mathbf{f}_C^H \mathbf{g}_n\right|^2 > \left(\sum_{i \in \mathcal{N} \setminus \{n\}} \left|\mathbf{f}_C^H \mathbf{g}_i\right| \right)^2$. Consequently, according to the Cauchy-Schwarz inequality [23], we have $(N-1) \sum_{i \in \mathcal{N} \setminus \{n\}} |\mathbf{f}_C^H \mathbf{g}_i|^2 \geq \left(\sum_{i \in \mathcal{N} \setminus \{n\}} |\mathbf{f}_C^H \mathbf{g}_i| \right)^2$. Using this result, we transform $|s_{SCS}| > |s_{\Sigma PCS}|$ into:

$$\left|\mathbf{f}_C^H \mathbf{g}_n\right|^2 > (N-1) \sum_{i \in \mathcal{N} \setminus \{n\}} \left|\mathbf{f}_C^H \mathbf{g}_i\right|^2. \tag{16}$$

As discussed in Lemma 2, we adopt $\mathbf{e}_M$ as $\mathbf{f}_C$. Then, according to the Rayleigh-Ritz theorem, $\mathbf{f}_C^H \mathbf{M} \mathbf{f}_C$ achieves its maximum value, $\mathbf{e}_M^H \mathbf{M} \mathbf{e}_M = \tau_M \|\mathbf{e}_M\|^2$, optimizing the quality of the synthesized covert signal. Additionally, based on the definition of $\mathbf{M}$ in Section IV-B, we have $\mathbf{e}_M^H \mathbf{M} \mathbf{e}_M = \left|\mathbf{e}_M^H \mathbf{g}_n\right|^2 - \eta \sum_{i \in \mathcal{N} \setminus \{n\}} \left|\mathbf{e}_M^H \mathbf{g}_i\right|^2$. Since $\mathbf{e}_M^H \mathbf{M} \mathbf{e}_M > 0$ holds, we can derive $|\mathbf{e}_M^H \mathbf{g}_n|^2 > \eta \sum_{i \in \mathcal{N} \setminus \{n\}} |\mathbf{e}_M^H \mathbf{g}_i|^2$. Consequently, comparing this inequality and Eq. (16) after replacing $\mathbf{f}_C$ with $\mathbf{e}_M$, we conclude that $|s_{SCS}| > |s_{\Sigma PCS}|$ satisfies when $\eta \geq N-1$.

Thus, Lemma 2 follows. ■

REFERENCES

[1] Y. Zou, J. Zhu, X. Wang, et al., "A Survey On Wireless Security: Technical Challenges, Recent Advances, and Future Trend," *Proc. IEEE*, vol. 104, no. 9, pp. 1727-1765, 2016.

[2] D. J. Bernstein and T. Lange, "Post-quantum cryptography," *Nature*, vol. 549, pp. 188–194, 2017.

[3] S. Yan and R. Malaney, "Location-Based Beamforming for Enhancing Secrecy in Rician Wiretap Channels," *IEEE Trans. Wireless Commun.*, vol. 15, no. 4, pp. 2780–2791, 2016.

[4] Q. Li and L. Yang, "Artificial Noise Aided Secure Precoding for MIMO Untrusted Two-Way Relay Systems With Perfect and Imperfect Channel State Information," *IEEE Trans. Inf. Foren. Sec.*, vol. 13, no. 10, pp. 2628–2638, 2018.

[5] R. A. Poisel, *Electronic Warfare Target Location Methods*. Norwood, MA, USA: Artech House, 2012.

[6] S. Yan, X. Zhou, J. Hu, et al., "Low Probability of Detection Communication: Opportunities and Challenges," *IEEE Wireless Commun.*, vol. 26, no. 5, pp. 19–25, 2019.

[7] B. A. Bash, D. Goeckel, and D. Towsley, "Limits of Reliable Communication With Low Probability of Detection on AWGN Channels," *IEEE J. Sel. Areas Commun.*, vol. 31, no. 9, pp. 1921–1930, 2013.

[8] P. H. Che, M. Bakshi, and S. Jaggi, "Reliable Deniable Communication: Hiding Messages in Noise," in *Proc. IEEE Int. Symp. Inf. Theory (ISIT)*, 2013, pp. 2945–2949.

[9] L. Wang, G. W. Wornell, and L. Zheng, "Fundamental Limits of Communication With Low Probability of Detection," *IEEE Trans. Inf. Theory*, vol. 62, no. 6, pp. 3493–3503, 2016.

[10] R. Soltani, D. Goeckel, D. Towsley, et al., "Covert Wireless Communication With Artificial Noise Generation," *IEEE Trans. Wireless Commun.*, vol. 17, no. 11, pp. 7252–7267, 2018.

[11] K. Shahzad, X. Zhou, S. Yan, et al., "Achieving Covert Wireless Communications Using a Full-Duplex Receiver," *IEEE Trans. Wireless Commun.*, vol. 17, no. 12, pp. 8517–8530, 2018.

[12] K. Shahzad, "Relaying via Cooperative Jamming in Covert Wireless Communications," in *Proc. Int. Conf. Signal Process. Commun. Syst. (ICSPCS)*, 2018, pp. 1–6.

[13] M. Forouzesh, P. Azmi, et al., "Covert Communication Using Null Space and 3D Beamforming: Uncertainty of Willie's Location Information," *IEEE Trans. Veh. Technol.*, vol. 69, no. 8, pp. 8568–8576, 2020.

[14] Z. Liu, J. Liu, Y. Zeng, et al., "On Covert Communication With Interference Uncertainty," in *Proc. IEEE Int. Conf. Commun. (ICC)*,2018, pp. 1–6.

[15] S. Ma, et al., "Robust Beamforming Design for Covert Communications," *IEEE Trans. Inf. Foren. Sec.*, vol. 16, pp. 3026–3038, 2021.

[16] Q. Li, D. Xu, K. Navaie, et al., "Covert and Secure Communications in NOMA Networks With Internal Eavesdropping," *IEEE Wireless Commun. Lett.*, vol. 12, no. 12, pp. 2178–2182, 2023.

[17] M. Schulz, A. Loch, and M. Hollick, "Practical Known-Plaintext Attacks against Physical Layer Security in Wireless MIMO Systems," in *Proc. Netw. Distrib. Syst. Secur. Symp. (NDSS)*, 2014.

[18] T. M. Cover and J. A. Thomas, *Elements of Information Theory*. Hoboken, NJ, US: Wiley, 2006.

[19] S. Fang, T. Wang, Y. Liu, et al., "Entrapment for Wireless Eavesdroppers," in *Proc. IEEE Conf. Comput. Commun. (INFOCOM)*, 2019, pp. 2530–2538.

[20] Y. Liu, Z. Li, K. G. Shin, et al., "iCoding: Countermeasure Against Interference and Eavesdropping in Wireless Communications," *IEEE Trans. Inf. Foren. Sec.*, vol. 19, pp. 9188–9203, 2024.

[21] Z. Li, L. Zhang, S. Le, et al., "Distributed Modulation Exploiting IRS for Secure Communications," *IEEE Trans. Mobile Comput.*, vol. 24, no. 10, pp. 11193–11208, 2025.

[22] R. A. Horn and C. R. Johnson, *Matrix Analysis*. New York, NY, USA: Cambridge University Press, 2012.

[23] J. M. Steele, *The Cauchy-Schwarz Master Class: An Introduction to the Art of Mathematical Inequalities*. New York, NY, USA: Cambridge University Press, 2004.